Vancouver Weather Dynamics Analysis: 2009-2019 Using Quantum Information Theory

Elsayed Barakat , Amr Youssef , Ibrahim El-Kalla , Montaser Qasymeh , Mahmoud Abdel-Aty *

Posted Date: 20 February 2025

doi: 10.20944/preprints202502.1645.v1

Keywords: Weather Dynamics; Quantum Information Theory; Entropy

 doi:10.20944/preprints202502.1645.v1

Article

Vancouver Weather Dynamics Analysis: 2009-2019 Using Quantum Information Theory

Elsayed Barakat [1], Amr Abd Al-Rahman Youssef [2], I.L. El-Kalla [1], M. Qasymeh [3] and M. Abdel-Aty [3,4,5,*]

[1] Mathematics and Engineering Physics Department, Faculty of Engineering, Mansoura University, Mansoura, Egypt
[2] PhD in Mathematics, (Free Scholar), Alexandria, Egypt; amraay2003@gmail.com
[3] Abu Dhabi University, Zayed City, MZ39, Abu Dhabi, United Arab Emirates; montasir.qasymeh@adu.ac.ae
[4] Deanship of Graduate Studies and Research, Ahlia University, P.O. Box 10878 Manama, Bahrain
[5] Mathematics Department, Faculty of Science, Sohag University, P.O. Box 82524, Sohag, Egypt
* Correspondence: mabdelaty@zewailcity.edu.eg

Abstract: In this paper, we analyze the weather dynamics in Vancouver, Canada from 2009-2019 using quantum information theory. The novel approach taken in this work demonstrates that applying quantum information principles to classical problems, such as weather analysis, can yield new features and valuable insights that would otherwise be overlooked. Historical data was examined using entropy, and coherence measures, revealing connections between quantum-level phenomena and macro-scale weather patterns. Key findings include the role of quantum coherence in weather shifts and evidence of quantum entanglement producing nonlinear weather dynamics. The results demonstrate the value of quantum information theory for enhancing weather forecasting and climate modeling.

Keywords: weather dynamics; quantum information theory; entropy

1. Introduction

In recent years, the climate lost regularity in cycles and became changeable to new states [1]. The climate changes occupied big areas with totally or partially damaging ecosystems [2]. Human societies must deal the climate problem with the slightest responsibility in order to protect the earth from negative changes [3].

Over the past two years, the heat dome has swept away, causing high temperatures and low humidity, accompanied by a lack of rainfall in the north of the Earth during the summers of 2022 and 2023, sparking forest fires in Canada, America, Britain, and on both sides of the Mediterranean in Spain, France, Italy, Greece, Turkey, Morocco, Algeria, and Tunisia. In Greenland, glaciers are melting rapidly. Summer continues for more weeks, autumn shortens, and winter progresses slowly and ends early, paving the way for spring to return quickly. The melting of ice and the separation of huge areas of it in Antarctica. The hurricanesanes increased, approaching 300 km/h, and became more ferocious and violent. There are many examples that cannot be enumerated here of the dire consequences that the Earth is currently witnessing in terms of climate change over the past two years. The suffering of human societies has increased around the world in the face of extreme climate. Difficult challenges have emerged, particularly water availability, due to disturbances in rainfall and the impact of extreme temperatures on agriculture. The environment became unhealthy due to human manipulation [4].

In this context, researchers from all over the world have rushed to study the climate changes in each region and their repercussions on the social and economic systems of human societies in developed and developing countries [5–8]. They made good efforts and distinguished contributions. They invented more effective devices to measure the weather in order to obtain accurate data about climate phenomena. They then established mathematical models describing various climate phenomena. Hence, they developed statistical, numerical and analytical methods in treating weather data and linked them to human activities to understand the repercussions of climate change [9–11].

In developing statistical, numerical, and analytical studies of various weather phenomena, there was, on the other hand, a new theory that began to become famous. Almost thirty years ago, the new

 doi:10.20944/preprints202502.1645.v1

theory about information systems was suggested as the quantum information theory. Its primary purpose was to build and operate a quantum computer. This theory developed in a parallel way and far from the issue of climate change in the world. With the spread of the issue of climate change, we were keen to develop techniques to understand the climate, so we sought the quantum information theory as a new mathematical method in studying weather data in addition to other methods currently used. The purpose here is to provide a new perspective in the study of climate variables and the interaction between them. There are quantum measures that are suitable for studying the climate.

In this manuscript we will investigate the Vancouver weather dynamics in the time domain from 2009 to 2019 by the aid of quantum mechanical measurements. The manuscript is arranged as follows; in section two we introduce the framework of the measurement technique and the preparing of the data to be suitable for it and we deduce the density matrix of the quantum system. In section three, we obtain the time evolution of the classical information, the quantum information, the decoherent information, Shannon entropy and von Neumann entropy monthly. Also, we recorded the maximum values of each case. In section four, we end with the conclusion.

2. The Mathematical Model

The novelty of this framework is configured to set up the quantum machine learning (QML) as the $d-$dimensional feature space F, of the dataset $\mathbb{X}$, in a viewpoit of the quantum information theory. Thus, we aim to formulate the dataset $\mathbb{X}$, in the quantum view. In the classical information system, the dataset $\mathbb{X}$, is provided as $n \times d$ matrix where n and d refers to the number of rows and number of columns respectively where x_{ij} is the numerical value in the dataset $\mathbb{X}$, $i = 1, 2, 3, ..., n$, and $j = 1, 2, 3, ..., d$. Therefore, the $d-$dimensional feature space F, is represented geometrically by the Hilbert space in the quantum framework where each feature represents a specific phenomenon provided in the standard basis vector. Consequently, the $d-$dimensional feature space F, is configured by standard bases $|c_1\rangle, |c_2\rangle, ..., |c_d\rangle$ where each column of $\mathbb{X}$ is represented by the standard basis and each row of $\mathbb{X}$ is formed by an arbitrary non-normalized vector $|r_i\rangle$, $i = 1, 2, 3, ..., n$. Hence, an arbitrary non-normalized vector $|r_i\rangle$ can be formed in terms of the standard bases $|c_1\rangle, |c_2\rangle, ..., |c_d\rangle$ as:

$$|r_i\rangle = \sum_{j=1}^{d} x_{ij}|c_j\rangle, \tag{1}$$

Hence, the vector $|r_i\rangle$ is normalized if it is taken in the form $|R_i\rangle$ as follows:

$$|R_i\rangle = \sum_{j=1}^{d} r_{ij}|c_j\rangle, \tag{2}$$

where $r_{ij} = x_{ij}/\sqrt{\sum_{j=1}^{d}|x_{ij}|^2}$ such that $\sum_{j=1}^{d}|r_{ij}|^2 = 1$. A given dataset $\mathbb{X}$, is defined on the set of real numbers $\mathbb{R}$ or the set of complex numbers $\mathbb{C}$ according to domains of x_{ij}'s elements. Indeed, the dataset $\mathbb{X}$, cannot be treated in the quantum mechanics, since it is not a square matrix. In this respect, the new quantum state ρ, is defined to describe $\mathbb{X}$, provided by the square matrix. The quantum state ρ, is the normailzed square matrix of order $d \times d$, and is introduced as:

$$\rho := \frac{\mathbb{X}^T\mathbb{X}}{tr(\mathbb{X}^T\mathbb{X})}. \tag{3}$$

which expressed in terms of standard bases $|c_1\rangle, |c_2\rangle, ..., |c_d\rangle$ as follows:

$$\rho = \sum_{i,j=1}^{d} \rho_{ij}|c_i\rangle\langle c_j|. \tag{4}$$

 doi:10.20944/preprints202502.1645.v1

where $\sum_{i=1}^{d} \rho_{ii} = 1$. The state ρ has three important facts. Firstly, it is always a mixed state. Hence, it has always a noise. Diagonal elements $\rho_{11}, \rho_{22}, ..., \rho_{dd}$ represent the classical information denoted by CI. CI is the information that can be directly observed, stored, and processed using traditional digital technologies. CI is investigated by:

$$CI = \sum_{n=1}^{d} \rho_n^2. \tag{5}$$

Non-diagonal elements $\rho_{ij}; i \neq j$, are the joint information of ket basis $|c_i\rangle$ and bra basis $\langle c_j|$, which describes the quantum information. These elements disappear in the classical information but exist in the quantum information theory. Hence, the quantum information theory forms a new type of the information which does not exist classically. QI is fundamentally different from CI which is due to the unique properties of quantum systems, such as superposition. QI is checked by:

$$QI = 2 \sum_{n=d+1}^{d(d-1)/2} |\rho_n|^2. \tag{6}$$

Clearly, two informaation terms CI and QI, yield the trace of ρ^2 which is written as:

$$Tr\rho^2 = CI + QI. \tag{7}$$

Hence, the new term is also defined as $1 - Tr\rho^2$, and is known as the linear entropy or purity. Here this term is named the decoherent information and denoted by DI. DI refers to the private information type that is not directly accessible or measurable with matrix elements like CI and QI. DI is detected by the relationship as:

$$DI = 1 - Tr\rho^2. \tag{8}$$

If ρ is the pure state, then the sum of CI and QI is equal to one and DI does not exist. Thus, Equation (7) becomes as follows:

$$CI + QI = 1. \tag{9}$$

If ρ is the mixed state, then the sum of CI and QI is less than one and there is a gap which forms the inequality in Equations (7) and (9). Therefore, a new term achieves the equality in the preceded inequality. DI describes a gap between one and the sum of CI and DI with using Equation (8) in what follows:

$$CI + QI + DI = 1. \tag{10}$$

The information has distinct realms, each with its own unique characteristics, and through which we can understand systems. The quantum information system can be divided into three different categories; CI, QI, and DI. According to the quantum informative view, the dataset $\mathbb{X}$, is manipulated by the formation of ρ, over the $d-$dimensional feature space F. Consequently, the quantum machine learning is defined here successfully.

To study the noise and the ambiguity of the information system, the entropy is used here to handle this mission. Indeed, the entropy is valid to measure the noise with a high accuracy. Shannon entropy is used to determine the noise of the classical information and is introduced as [12]:

$$S_H = -\sum_{i}^{d} \rho_i \log_d \rho_i. \tag{11}$$

where $S_H > 0$, and depends on the diagonal terms of ρ. S_H always exists for all cases of ρ. von Neumann entropy is a precise and widely-used quantum measure due to its strong theoretical foundations and it

 doi:10.20944/preprints202502.1645.v1

is also known as nonlinear entropy. It is a quantum analogues of the classical Shannon entropy and is introduced as [13]:

$$S_N = -\sum_{i}^{d} \lambda_i \log_d \lambda_i \tag{12}$$

where λ_i is the eigenvalue of the quantum state ρ. von Neumann entropy can be applied to any quantum state, whether pure or mixed, and is not limited to particular systems or states. This makes it a versatile and widely applicable quantum measure. Consequently, $S_N = 0$, if ρ is a pure state and $S_N > 0$, if ρ is a mixed state. Hence, S_N measures the noise of the decoherent information.

3. Quantum Weather Model

In this setting, we propose this novel technique to investigate the weather dynamics in Canada as a good exercise. Climate changes in Canada are in the spotlight here. Canada characterizes a wide range of both of geological and meteorological regions. It has a cold continental climate with winters lasting for six months and heavy snow falls, covering vast areas. In addition, the rainfall falls with great annular rates over all provinces and territories. Temperatures vary in the summer from a region to a region [14–17]. Thus, no one can study totally the climate in Canada. Therefore, the study is focused on a local region like Vancouver city. Some of basic information is provided about the geography and the climate of Vancouver city. Vancouver is a major city in western Canada, located in the Lower Mainland region of British Columbia province. It lies between Burrard Inlet to the north and the Fraser River to the south. The Strait of Georgia, to the west, is shielded from the Pacific Ocean by Vancouver Island. It is one of Canada's warmest cities in the winter. Vancouver's climate is temperate by Canadian standards and is marine west coast. In the summer, it is dry [18].

Vancouver weather dataset is investigated by the weather dataset as an example for the QML. The dataset is formed of ten weather variables and 4017 records from on January 2009 to 31^{th} December 2019 [19]. Here, names of weather variables are the maximum temperature (K), the minimum temperature (K), the dew point (K) where K is Keliven, the cloudcover (%), the humidity (%), the precipitation (mm), the total Snow (cm), the pressure (bar), the wind direction degree, and the wind speed (km/h) respectively.

In this setting, consider the quantum ten-dimensional feature space of bases $|c_1\rangle$, $|c_2\rangle$, ..., and $|c_{10}\rangle$, to represent the weather model with this novel technique. Weather vraiables are formulated in the quantum ten-dimensional feature space as the maximum temperature $|c_1\rangle$, the minimum temperature $|c_2\rangle$, the dew point $|c_3\rangle$, the cloudcover $|c_4\rangle$, the humidity $|c_5\rangle$, the precipitation $|c_6\rangle$, the total Snow $|c_7\rangle$, the pressure $|c_8\rangle$, the $x-$wind speed $|c_9\rangle$, and the $y-$wind speed $|c_{10}\rangle$, where the wind speed and the wind direction are solved into the $x-$wind speed and the $y-$wind speed respectively.

Thus, an arbitrary instance pure weather state $|w_i\rangle$ gives the numerical data of the $i-$row in the weather dataset $\mathbb{W}$ and can be written as:

$$|w_i\rangle = \sum_{j=1}^{10} w_{ij}|c_j\rangle. \tag{13}$$

where w_{ij}'s are real values. The daily quantum weather state is symbolized as $|d, m, y\rangle$ where d is the day order in the month, m is the month order, and y is the year. If the date is 03/01/2009, then the corresponding daily quantum weather state of the same date is written as $|03, 01, 2009\rangle$. Consequently with using Equations (1) and (13), the quantum daily weather state $|03, 01, 2009\rangle$ can be described by a numerical data in terms of ten bases as follows:

$$\begin{aligned} |03, 01, 2009\rangle \quad = \quad & 275|c_1\rangle + 271|c_2\rangle + 272|c_3\rangle + 82|c_4\rangle + 96|c_5\rangle \\ & +2.2|c_6\rangle + 0.8|c_7\rangle + 1021|c_8\rangle - 6.35|c_9\rangle + 12.47|c_{10}\rangle \end{aligned} \tag{14}$$

where the state $|03, 01, 2009\rangle$ gives the data record in Vancouver weather dataset.

 doi:10.20944/preprints202502.1645.v1

Table 1. Maximum reference of Vancouver weather.

Varaible	Max Ref	Varaible	Max Ref	Varaible	Max Ref
MaxTemp (K)	301	CloudCover (%)	100	TotalSnow (cm)	8.2
MinTemp (K)	294	Humidity (%)	99	Pressure (bar)	1044
DewPoint (K)	291	Precip (mm)	78.7	Wind (km/h)	36

It is obvious that the daily quantum weather state is unbalance because of all data have distinct units. Therefore, it necessary that all data is reformed in dimensionless data in order to be balanced. To achieve this aim, the maximum reference of each column is calculated from 01/01/2009 to 31/12/2019 in the Vancouver weather dataset on the data in Table 1. In the maximum reference (Max- Ref) approach, the daily quantum weather state $|03, 01, 2009\rangle$ can be reformed in dimensionless data where each value of a weather variable is divided by the corresponding maximum reference value of the same weather variable as in Table 1, in what follows:

$$\begin{aligned} |03, 01, 2009\rangle_{Max\_Ref} &= 0.9136\,|c_1\rangle + 0.9217\,|c_2\rangle + 0.9347|c_3\rangle + 0.82\,|c_4\rangle + 0.9697|c_5\rangle \\ &\quad +0.0279\,|c_6\rangle + 0.0976|c_7\rangle + 0.9779|c_8\rangle - 0.1765\,|c_9\rangle + 0.3465|c_{10}\rangle \end{aligned} \tag{15}$$

where Equation (15) is non-normalized. In subsequent by Equation (2), the state $|03, 01, 2009\rangle_{Max\_Ref}$ becomes normalized as:

$$\begin{aligned} |03, 01, 2009\rangle_{Max\_Ref\_N} &= 0.3973\,|c_1\rangle + 0.4008\,|c_2\rangle + 0.4064|c_3\rangle + 0.3566\,|c_4\rangle + 0.4217|c_5\rangle \\ &\quad +0.0122\,|c_6\rangle + 0.0424|c_7\rangle + 0.4253|c_8\rangle - 0.0768\,|c_9\rangle + 0.1507|c_{10}\rangle \end{aligned} \tag{16}$$

Actually, the daily quantum weather state $|03, 01, 2009\rangle_{Max\_Ref\_N}$ is pure normalized. Each numerical value of dimensionaless weather variable is affected by other values of all variables using the normailzation constant. All same computations are established over all instance weather states in this statistics to obtain normalized quantum pure daily weather states. According to the statistics, we have 4017 normalized daily quantum pure weather states from 01/01/2009 to 31/12/2019.

How to construct the state ρ over an arbitrary date interval from the $i-$row to the $j-$row, the first step, the weather dataset $\mathbb{W}$, is modified into a new formalism which each column is divided by the corresponding maximum reference according to Table 1. Thus, the new dimensionless weather dataset $\mathbb{S}$ is built. The second step, the state $\rho(i:j)$ from the $i-$row to the $j-$ row is computed by Equation (3) as:

$$\rho(i:j) = \frac{\mathbb{S}^T(i:j)\mathbb{S}(i:j)}{tr(\mathbb{S}^T(i:j)\mathbb{S}(i:j))}. \tag{17}$$

This statistics is partitioned according to months. Thus, there are 132 covariance matrices $\mathbb{S}(1:31)$, $\mathbb{S}(32:59)$, ..., $\mathbb{S}(3957:3986)$, and $\mathbb{S}(3987:4017)$, which correspond to $1/2009, 2/2009, ..., 11/2019$, and $12/2019$, respectively. The monthly quantum state $\rho(1/2009)$ is determined from 01/01/2009 to 31/12/2009, by Equation (17):

$$\rho(1/2009) = \frac{\mathbb{S}^T(1:31)\mathbb{S}(1:31)}{tr(\mathbb{S}^T(1:31)\mathbb{S}(1:31))}. \tag{18}$$

and the corresponding matrix of $1/2009$ is computed as:

 doi:10.20944/preprints202502.1645.v1

$$\rho(1/2009) = \begin{bmatrix} 0.1780 & 0.1798 & 0.1816 & 0.0950 & 0.1633 & 0.0058 & 0.0071 & 0.1894 & -0.0162 & 0.0225 \\ 0.1798 & 0.1817 & 0.1835 & 0.0963 & 0.1651 & 0.0059 & 0.0072 & 0.1914 & -0.0165 & 0.0227 \\ 0.1816 & 0.1835 & 0.1853 & 0.0974 & 0.1669 & 0.0060 & 0.0073 & 0.1933 & -0.0167 & 0.0228 \\ 0.0950 & 0.0963 & 0.0974 & 0.0764 & 0.0943 & 0.0059 & 0.0072 & 0.1010 & -0.0157 & 0.0148 \\ 0.1633 & 0.1651 & 0.1669 & 0.0943 & 0.1532 & 0.0061 & 0.0074 & 0.1737 & -0.0175 & 0.0198 \\ 0.0058 & 0.0059 & 0.0060 & 0.0059 & 0.0061 & 0.0008 & 0.0008 & 0.0061 & -0.0017 & 0.0015 \\ 0.0071 & 0.0072 & 0.0073 & 0.0072 & 0.0074 & 0.0008 & 0.0056 & 0.0075 & -0.0021 & 0.0036 \\ 0.1894 & 0.1914 & 0.1933 & 0.1010 & 0.1737 & 0.0061 & 0.0075 & 0.2016 & -0.0171 & 0.0240 \\ -0.0162 & -0.0165 & -0.0167 & -0.0157 & -0.0175 & -0.0017 & -0.0021 & -0.0171 & 0.0059 & -0.0027 \\ 0.0225 & 0.0227 & 0.0228 & 0.0148 & 0.0198 & 0.0015 & 0.0036 & 0.0240 & -0.0027 & 0.0114 \end{bmatrix}. \quad (19)$$

Elements of the state $\rho(1/2009)$ expresses for the classical information which appear in diagonal elements and the quantum information which appear in non-diagonal elements. In fact, each element matrix is influenced by all weather dimensionaless variables because of the term $tr(S^T(1:31)S(1:31))$. Vancouver ether dataset is checked later by quantum informative measurements (the classical information, the quantum information, the decoherent information, Shannon entropy and von Neumann entropy).

4. Discussion and Results

In order to study the climate, one needs to visualize the time evolution of the climate variables and we can get a comprehensive understanding of each one of them. This allows us to detect extremes, trends, and the overall climate characteristics. Figure 1, shows the time evolution of each climate variable. Figures 1a and 1c, presents the evolution of the maximum temperature, minimum temperature, and dew point in Keliven. It is clear that we have a cyclic evolution yearly, whereas the maximum of each cycle is reached in the half of each year and the minimum is recorded at the beginning and the end of each year. Indeed, the cloud cover and humidity percentage have no cyclic evolution as shown in Figure 2a,2b. If we look insight, we can detect a trend of increase in the maximum precipitation values with an extreme values in 2015 as shown in Figure 2c. Figure 3b presents a roughly oscillation without any cyclic evolution whereas the mean values are approximately constant. Snow is a discrete time phenomena happening per year, so as in Figure 3a, total snow is recorded in between sequential two years. Indeed the total snow has its extreme in 2016 and 2017. In Figure 3c, wind speed has a cyclic evolution with fluctuations in each year. Also, the minimum value are approximately stationary with respect to the variation in the maximum values.

In this analysis of a time evolution in the feature space, the classical information CI, the quantum information QI, the decoherent information DI, Shannon entropy and von Neumann entropy are plotted against the months as the time units from Jan/2009 into Dec/2021. Information has distinct realms, each with its own unique characteristics, and through which we can understand systems.

The classical information, the quantum information, the decoherent information, Shannon entropy and von Neumann entropy are computed for monthly mixed states by Equations (5), (6), (8), (11), (12), (17), (18), (19), and all numerical values are mentioned in tables. Tables 2–6 refer to the classical information, the quantum information, the decoherent information, Shannon entropy and von Neumann entropy rerspcetively. Each table includes 132 numerical values refers to years from 2009 to 2019 vertically and to months horizontally from January to December.

In Table 2, values of CI provide the effect individually of each weather variable of a range $[0.1567, 0.2012]$. In Table 3, values of QI describe the mutual interaction of pair of two variables of a range $[0.7296, 0.8023]$. Obviously, QI values enlarge comparison with values of CI. Therefore, the effect of QI is greater than the effect of CI in this system. In Table 4, DI values are small relative to QI and CI and has a range $[0.0090, 0.0882]$. In Table 5, S_H values describe the classical noise of CI and is ranged by $[0.7201, 0.8368]$. in Table 6, S_N values describe the noise of DI of a range $[0.0147, 0.1172]$. It noted that S_N values weaken relative to S_H values.

 doi:10.20944/preprints202502.1645.v1

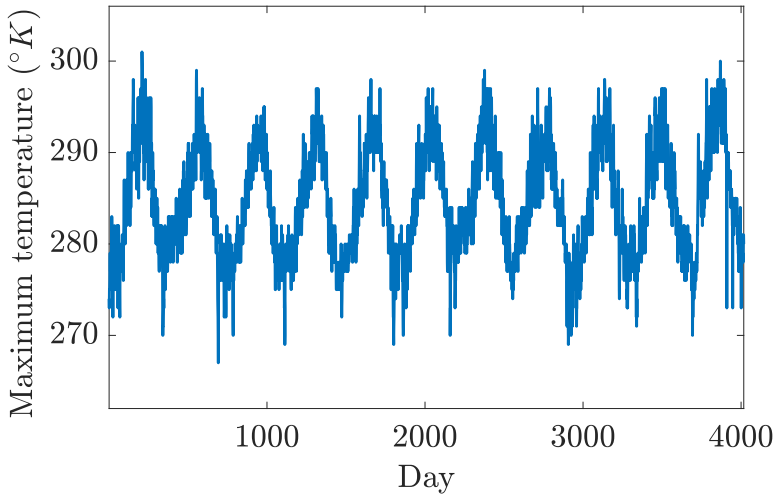

(a) Maximum temperature

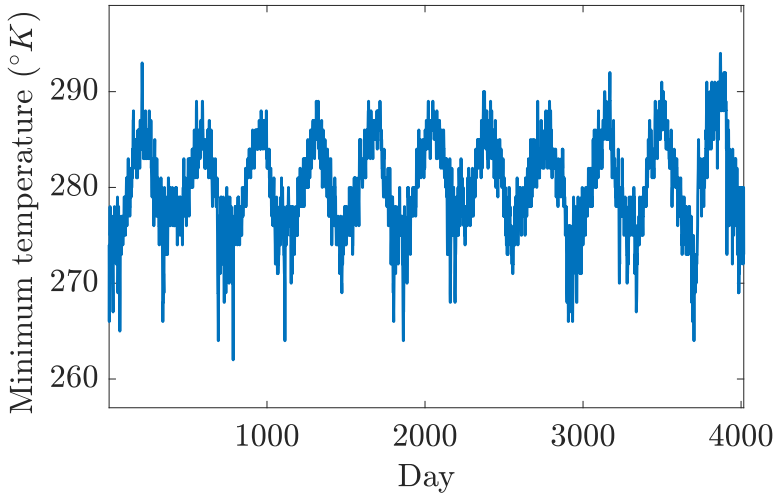

(b) Minimum temperature

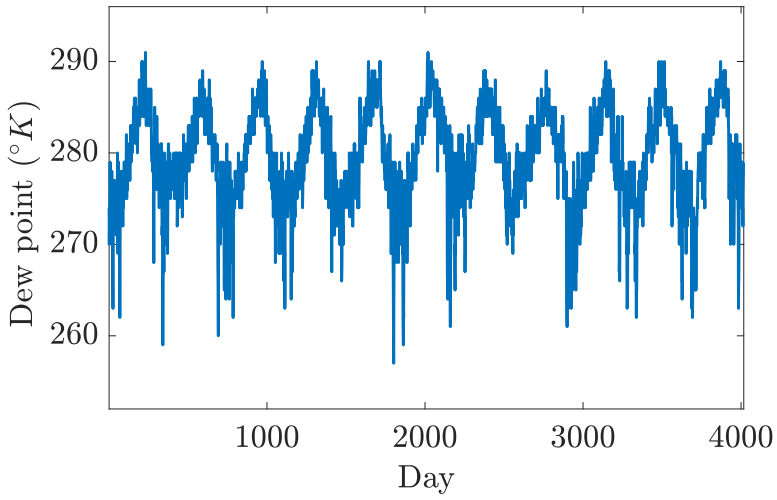

(c) Dew point

Figure 1. Vancouver weather variables; maximum temperature, minimum temperature, and dew point. (a) Maximum temperature; (b) Minimum temperature; (c) Dew point.

 doi:10.20944/preprints202502.1645.v1

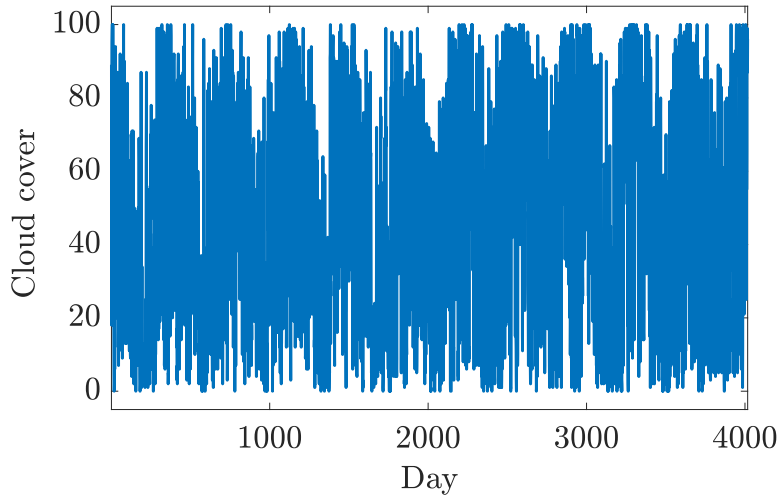

(a) Cloud cover

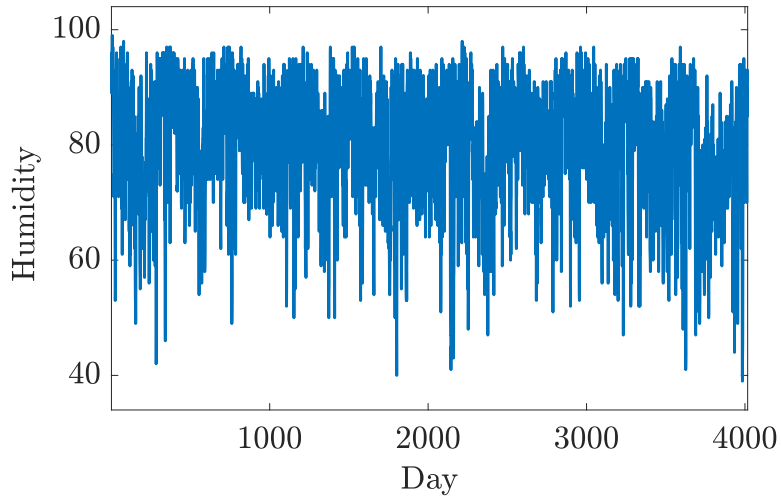

(b) Humidity

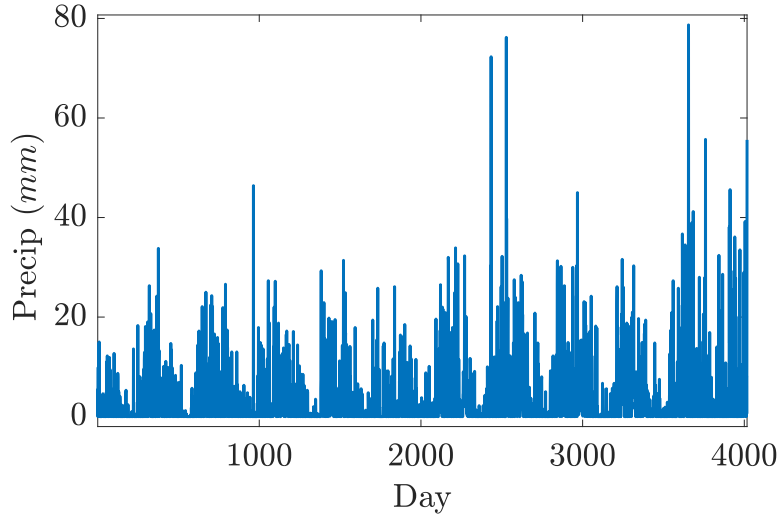

(c) Precipitation

Figure 2. Vancouver weather variables; cloud cover, humidity, and precipitation.

Preprints.org (www.preprints.org) | NOT PEER-REVIEWED | Posted: 20 February 2025 doi:10.20944/preprints202502.1645.v1

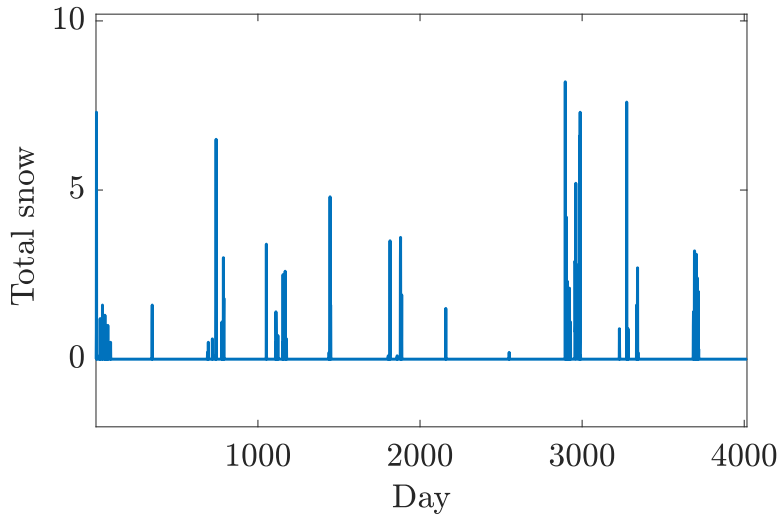

(a) Total snow

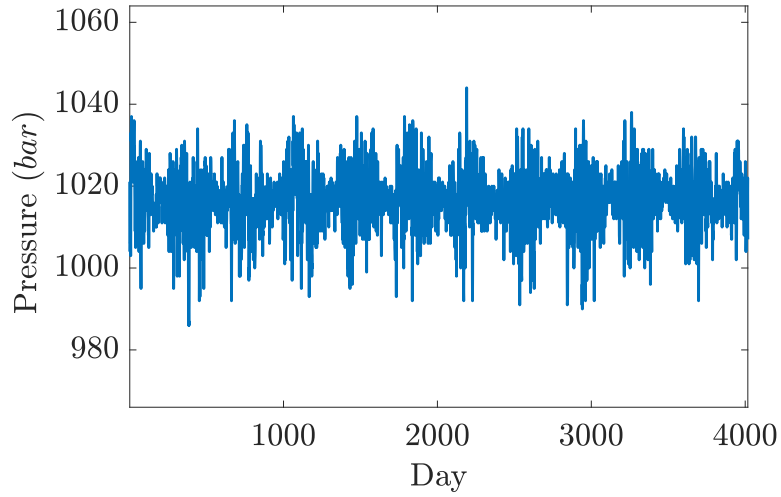

(b) Pressure

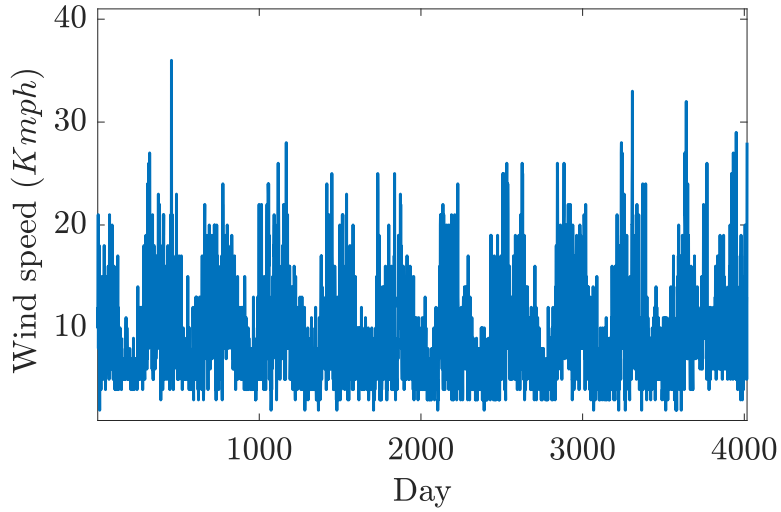

(c) Wind speed

Figure 3. Vancouver weather variables; total snow, pressure, and wind speed.

 doi:10.20944/preprints202502.1645.v1

Table 5. Shannon Entropy of Monthly States.

	Jan	Feb	Mar	Apr	May	Jun	Jul	Aug	Sep	Oct	Nov	Dec
2009	0.8045	0.7935	0.8068	0.7805	0.7201	0.7517	0.7383	0.7369	0.7691	0.8080	0.7926	0.8128
2010	0.7820	0.8169	0.8176	0.8139	0.7940	0.7731	0.7345	0.7365	0.7648	0.7670	0.8032	0.7651
2011	0.8000	0.7945	0.8122	0.7870	0.8040	0.7415	0.7553	0.7685	0.7610	0.7664	0.7439	0.8071
2012	0.7660	0.7931	0.8089	0.8221	0.8241	0.7840	0.7960	0.7624	0.7447	0.7374	0.7706	0.7530
2013	0.7584	0.7990	0.8157	0.8018	0.7856	0.7935	0.8023	0.7827	0.7662	0.7268	0.7337	0.7615
2014	0.7410	0.7774	0.7885	0.8150	0.8034	0.7826	0.8049	0.8015	0.8156	0.7566	0.7451	0.7760
2015	0.7274	0.7640	0.7790	0.7864	0.7938	0.8057	0.7923	0.8368	0.8248	0.7808	0.7843	0.7629
2016	0.7390	0.7257	0.7613	0.7619	0.7840	0.8012	0.8001	0.8043	0.8315	0.8347	0.7769	0.8018
2017	0.7498	0.7453	0.7519	0.7757	0.7673	0.7839	0.7977	0.8077	0.8068	0.8056	0.8060	0.8102
2018	0.7912	0.7709	0.7434	0.7467	0.7580	0.7624	0.7722	0.8180	0.8206	0.8324	0.8342	0.7870
2019	0.8314	0.7825	0.7666	0.7314	0.7152	0.7529	0.7504	0.7767	0.8374	0.8119	0.8079	0.8214

Table 2. Classical Information CI of Monthly States.

	Jan	Feb	Mar	Apr	May	Jun	Jul	Aug	Sep	Oct	Nov	Dec
2009	0.1693	0.1734	0.1681	0.1784	0.2002	0.1879	0.1935	0.1963	0.1820	0.1655	0.1718	0.1683
2010	0.1765	0.1625	0.1636	0.1674	0.1725	0.1817	0.1940	0.1956	0.1835	0.1828	0.1679	0.1877
2011	0.1704	0.1717	0.1655	0.1762	0.1681	0.1951	0.1880	0.1853	0.1836	0.1823	0.1924	0.1714
2012	0.1839	0.1727	0.1693	0.1626	0.1612	0.1754	0.1726	0.1838	0.1918	0.1950	0.1816	0.1912
2013	0.1871	0.1721	0.1642	0.1694	0.1735	0.1722	0.1720	0.1751	0.1820	0.1987	0.1976	0.1884
2014	0.1946	0.1790	0.1748	0.1650	0.1672	0.1775	0.1694	0.1717	0.1635	0.1870	0.1918	0.1825
2015	0.1996	0.1832	0.1771	0.1737	0.1730	0.1724	0.1714	0.1568	0.1598	0.1797	0.1753	0.1878
2016	0.1936	0.2003	0.1845	0.1864	0.1769	0.1689	0.1676	0.1678	0.1610	0.1571	0.1790	0.1723
2017	0.1905	0.1911	0.1882	0.1783	0.1823	0.1766	0.1701	0.1656	0.1692	0.1694	0.1683	0.1701
2018	0.1749	0.1806	0.1922	0.1896	0.1856	0.1840	0.1816	0.1641	0.1647	0.1567	0.1592	0.1765
2019	0.1583	0.1781	0.1843	0.1959	0.2012	0.1877	0.1891	0.1783	0.1567	0.1660	0.1683	0.1597

Table 3. Quantum Information QI of Monthly States.

	Jan	Feb	Mar	Apr	May	Jun	Jul	Aug	Sep	Oct	Nov	Dec
2009	0.7454	0.7535	0.7692	0.7788	0.7802	0.7836	0.7780	0.7655	0.7662	0.7866	0.7874	0.7486
2010	0.7786	0.7839	0.7706	0.7589	0.7555	0.7676	0.7863	0.7671	0.7848	0.7735	0.7648	0.7584
2011	0.7681	0.7778	0.7674	0.7604	0.7819	0.7659	0.7655	0.7563	0.7878	0.7661	0.7830	0.7367
2012	0.7742	0.7823	0.7596	0.7750	0.7820	0.7715	0.7888	0.7711	0.7657	0.7778	0.7772	0.7677
2013	0.7730	0.7604	0.7979	0.7711	0.7694	0.7661	0.7326	0.7752	0.7693	0.777	0.7685	0.7702
2014	0.7777	0.7751	0.7760	0.7799	0.7959	0.7564	0.7569	0.7449	0.7926	0.7702	0.7638	0.7676
2015	0.7709	0.7930	0.7917	0.7965	0.7584	0.7395	0.7798	0.7719	0.8023	0.7528	0.7642	0.7660
2016	0.7769	0.7790	0.7971	0.7734	0.7772	0.7811	0.7657	0.7731	0.7368	0.7818	0.7541	0.7519
2017	0.7743	0.7746	0.7909	0.7980	0.7769	0.7819	0.7828	0.7876	0.7498	0.7448	0.7591	0.7296
2018	0.7544	0.7822	0.7815	0.7815	0.7895	0.7907	0.7772	0.7637	0.7614	0.7830	0.7556	0.7431
2019	0.7800	0.7681	0.7625	0.7850	0.7899	0.7898	0.7786	0.7843	0.7876	0.7601	0.7559	0.7887

Table 4. Decoherent Information DI of Monthly States.

	Jan	Feb	Mar	Apr	May	Jun	Jul	Aug	Sep	Oct	Nov	Dec
2009	0.0855	0.0733	0.0629	0.0430	0.0198	0.0287	0.0286	0.0383	0.0520	0.0480	0.041	0.0832
2010	0.0451	0.0537	0.0659	0.0738	0.0722	0.0509	0.0199	0.0375	0.0319	0.0438	0.0674	0.054
2011	0.0617	0.0507	0.0672	0.0635	0.0501	0.0392	0.0467	0.0586	0.0288	0.0518	0.0248	0.0921
2012	0.0421	0.0452	0.0712	0.0626	0.0569	0.0533	0.0387	0.0452	0.0427	0.0274	0.0413	0.0412
2013	0.0400	0.0677	0.038	0.0597	0.0573	0.0619	0.0956	0.0499	0.0489	0.0245	0.0341	0.0416
2014	0.0279	0.0461	0.0493	0.0553	0.0371	0.0663	0.0738	0.0836	0.0440	0.0429	0.0446	0.0501
2015	0.0296	0.0239	0.0314	0.0300	0.0688	0.0882	0.049	0.0715	0.0381	0.0677	0.0606	0.0464
2016	0.0296	0.0209	0.0186	0.0403	0.0461	0.0501	0.0668	0.0592	0.1023	0.0612	0.0670	0.0759
2017	0.0353	0.0344	0.0211	0.0238	0.0409	0.0417	0.0472	0.047	0.0812	0.086	0.0727	0.1005
2018	0.0708	0.0373	0.0265	0.0291	0.0251	0.0255	0.0414	0.0723	0.0741	0.0604	0.0854	0.0805
2019	0.0618	0.0539	0.0533	0.0192	0.0090	0.0226	0.0324	0.0375	0.0558	0.0740	0.0759	0.0518

Table 6. von Neumann Entropy of Monthly States.

	Jan	Feb	Mar	Apr	May	Jun	Jul	Aug	Sep	Oct	Nov	Dec
2009	0.0993	0.0838	0.0770	0.0539	0.0289	0.0372	0.0373	0.0473	0.0621	0.0592	0.0530	0.1014
2010	0.0572	0.0670	0.0796	0.0874	0.0812	0.0611	0.0274	0.0465	0.0418	0.0541	0.0793	0.0681
2011	0.0757	0.0625	0.0832	0.0764	0.0621	0.0503	0.0579	0.0685	0.0361	0.0602	0.0338	0.1016
2012	0.0549	0.0575	0.0877	0.0769	0.0721	0.0662	0.0500	0.0539	0.0519	0.0368	0.0511	0.0517
2013	0.0514	0.0798	0.0512	0.0743	0.0675	0.0754	0.1061	0.0621	0.0577	0.0331	0.0441	0.0522
2014	0.0381	0.0572	0.0596	0.0699	0.0483	0.0773	0.0874	0.0968	0.0571	0.0531	0.0526	0.0617
2015	0.0390	0.0324	0.0414	0.0404	0.0808	0.1011	0.0605	0.0884	0.0514	0.0787	0.0703	0.0574
2016	0.0379	0.0299	0.0265	0.0512	0.0582	0.0636	0.0782	0.0721	0.1172	0.0754	0.0752	0.0894
2017	0.0463	0.0436	0.0290	0.0324	0.0512	0.0524	0.0595	0.0589	0.0935	0.1010	0.0849	0.1131
2018	0.0843	0.0472	0.0358	0.0362	0.0340	0.0346	0.0517	0.0846	0.0925	0.0754	0.1001	0.0927
2019	0.0751	0.0642	0.0639	0.0273	0.0147	0.0301	0.0415	0.0480	0.0723	0.0896	0.0882	0.0676

 doi:10.20944/preprints202502.1645.v1

In order to predict quantum informative measures for proceeding years, the time evolution of quantum informative measures can be categorized by oscillating forms for the monthly evolution. We can adopt the time series function like Fourier series as a fitted function to express for quantum informative measures of the time t which takes the form:

$$f(t) = A_0 + \sum_{n=1}^{10} (A_n \cos(\frac{\pi}{12} nt) + B_n \cos(\frac{\pi}{12} nt)). \tag{20}$$

where the time unit is the month and varies from 1 to 156 to express for years from 2009 to 2021. Also, $A_0, A_1, ..., A_{10}, B_1, B_2, ..., B_{10}$ are real parameters which are detemined by the fitting curve method. The fitting curve method is applied from 2009 to 2017 where $t = 1, 2, ..., 108$, and we compare predicated results with computational values in Table 2–6 from 2018 and 2019, where $t = 109, 110, 111, ..., 132$. Hence, we predict values for each quantum informative measure for 2020 and 2021, where $t = 133, 134, ..., 156$. Parameters of Equation (20) are determined In Table 7 for CI, QI, DI, S_H and S_N.

Table 7. Parameters of Equation (20) for, S_N, S_H, CI, QI, and DI, of Monthly States.

Parameter	v. N. entropy	Shannon entropy	CI	QI	DI
A_0	0.177419252	0.771902703	0.050678047	0.062049865	0.781987886
A_1	-0.000158677	4.66897E-05	0.000111989	-5.08322E-05	0.000275487
A_2	-0.011405366	-0.007858178	0.019263546	0.021589135	0.030023996
A_3	-0.000721583	-0.000557379	0.001278965	0.00131916	0.00230835
A_4	-0.000275198	0.000418487	-0.000143289	-0.000220944	0.000743881
A_5	-2.12737E-05	-0.001728215	0.001749489	0.001714854	0.000457247
A_6	0.000229768	-0.000917736	0.000687968	0.000690732	-0.000686796
A_7	0.000360973	-0.001229884	0.000868912	0.000911237	-0.000443432
A_8	-0.001239609	0.001013982	0.000225626	0.000555403	0.003133055
A_9	-0.000768555	0.000722267	4.62848E-05	0.000205189	0.002148372
A_{10}	0.001041466	-0.001634011	0.000592543	0.000879101	-0.002190341
B_1	0.000885263	-0.003085051	0.002199789	0.002558227	-0.000869759
B_2	-0.006672415	0.001702886	0.004969532	0.00636236	0.017017788
B_3	0.000206905	-0.001544597	0.001337692	0.00162192	-0.000179637
B_4	0.002695816	0.000630608	-0.003326422	-0.003437865	-0.00736565
B_5	0.001116448	-0.001813767	0.000697323	0.000709658	-0.003130208
B_6	0.001073933	-0.00121763	0.0001437	-9.35565E-05	-0.003256093
B_7	-0.000321005	-0.000170955	0.000491964	0.000328852	0.000643332
B_8	-0.000217418	4.09508E-05	0.000176467	-0.000110103	0.000331478
B_9	0.000229142	-0.001453441	0.0012243	0.00108596	-0.000182739
B_{10}	0.000410576	0.000986727	-0.0013973	-0.001488531	-0.001025396

Table 8 presents a comprehensive analysis of the statistical parameters for predicted data CI, QI, DI, S_H, and S_N based on data from 2009 to 2019. The parameters evaluated include maximum error $E_{\max}$, average error E_{avg},minimum error $E_{\min}$, standard deviation σ and Pearson correlation P. Among the models, CI demonstrates the lowest errors, with $E_{\max} = 0.0181$ and $E_{avg} = 0.0044$, indicating more consistent predictions with minimal deviation. Conversely, Shannon entopy shows the highest errors, with $E_{\max} = 0.0437$ and $E_{avg} = 0.0115$. The minimum error values across all models are in the range of 10^{-5} with CI having the lowest at $4.23068 \times 10^{-6}$and Shannon entropy the highest at 1.76316×10^{-5}. The standard deviation, which reflects the spread of prediction errors, is lowest for CI at 0.0036 and highest for S_Pred at 0.0092, reinforcing the observation that CI offers more stable predictions. In terms of performance accuracy, CI scores the highest with P at 0.8619, indicating superior reliability, while QI has the lowest accuracy at 0.4705. Overall, the table suggests that CI outperforms the other models in terms of error minimization and prediction accuracy, making it the most reliable among the five models analyzed.

Table 8. Statistical parameters of the predicted data from 2009 to 2019.

	CI_Pred	QI_Pred	DI_Pred	S_H_Pred	S_N_Pred
$E_{\max}$	0.018078962	0.036793858	0.040334208	0.043658586	0.04026238
E_{avg}	0.0044402	0.010347299	0.010444764	0.01148774	0.010795253
$E_{\min}$	4.23068×10^{-6}	6.41655×10^{-5}	2.80891×10^{-5}	1.76316×10^{-5}	4.56022×10^{-5}
σ	0.003599035	0.007706359	0.007902501	0.00919112	0.008122923
P	0.861855921	0.470495165	0.743155671	0.864809389	0.771715928

 doi:10.20944/preprints202502.1645.v1

In Table 9, all predicted values of each quantum informative measure are recorded from 2020 to 2021 based on months from $t = 133, 134, 135, ..., 156$.

Table 9. Predicted values from 2020 to 2021.

Month	CI_Pred	QI_Pred	DI_Pred	S_H_Pred	S_N_Pred
Jan-20	0.166124748	0.772747654	0.061127595	0.809611216	0.074341245
Feb-20	0.168446307	0.768341842	0.063211852	0.805704921	0.076655972
Mar-20	0.168622351	0.778013189	0.053364471	0.803293507	0.066196118
Apr-20	0.17382895	0.777993988	0.04817706	0.789534882	0.059371264
May-20	0.184168249	0.777478934	0.038352821	0.764126107	0.048341799
Jun-20	0.183693624	0.788381804	0.02792457	0.763364364	0.036822284
Jul-20	0.191687926	0.779258913	0.029053148	0.744118694	0.037460586
Aug-20	0.194304217	0.774533696	0.031162091	0.736327212	0.039535831
Sep-20	0.183543641	0.772779172	0.043677184	0.763686139	0.053477581
Oct-20	0.174805326	0.77128455	0.053910124	0.788238257	0.064185118
Nov-20	0.165508032	0.769352677	0.065139284	0.813539223	0.077692965
Dec-20	0.164461197	0.760178725	0.075360079	0.817757705	0.089642898
Jan-21	0.168298361	0.761099208	0.070602458	0.805068914	0.083394425
Feb-21	0.169861336	0.768636116	0.061502553	0.801521056	0.076030359
Mar-21	0.169615786	0.774797693	0.055586519	0.803957581	0.069391076
Apr-21	0.176033828	0.772254773	0.051711402	0.785940236	0.062669229
May-21	0.184786524	0.77560273	0.039610744	0.763327374	0.04994273
Jun-21	0.188383529	0.77910839	0.032508083	0.754071564	0.041628431
Jul-21	0.194080219	0.775640391	0.030279391	0.740007288	0.03915999
Aug-21	0.190186498	0.77527685	0.034536655	0.749980849	0.043780673
Sep-21	0.184037584	0.764402739	0.051559675	0.766571011	0.062240072
Oct-21	0.177946779	0.76116993	0.060883291	0.783147933	0.072832637
Nov-21	0.168557599	0.761659131	0.069783269	0.806547581	0.082959794
Dec-21	0.16707943	0.765671768	0.067248801	0.808265656	0.081443686

Each quantum informative measure investigates monthly mixed weather states. In all figures, each quantum informative measure is plotted versus the months as the unit time from 1 to 156 where the month domain $[1, 132]$ provides the computational values and the month domain $[1, 156]$ presents predicted values, especially future predicted values from 133 to 156. The blue curve represents computational values and the red curve shows predicted values. The shaded area on the right figure during the period $[133, 156]$ marks the prediction period for 2020 and 2021. Predicated curves are plotted by Equation (20) and Tables (7,9). All curves are taken in waveforms.

Figures 4–6 show a comparison between three distinct types of the information; CI, QI, and DI, respectively. In Figure 4, the classical information is plotted by Tables 2, 7 and 8 and Equation (20) versus months in two curves. Two curves are close in nearly sinusoidal forms with a cyclic behavior. It has maximum extremes in summer and minimum in winter.

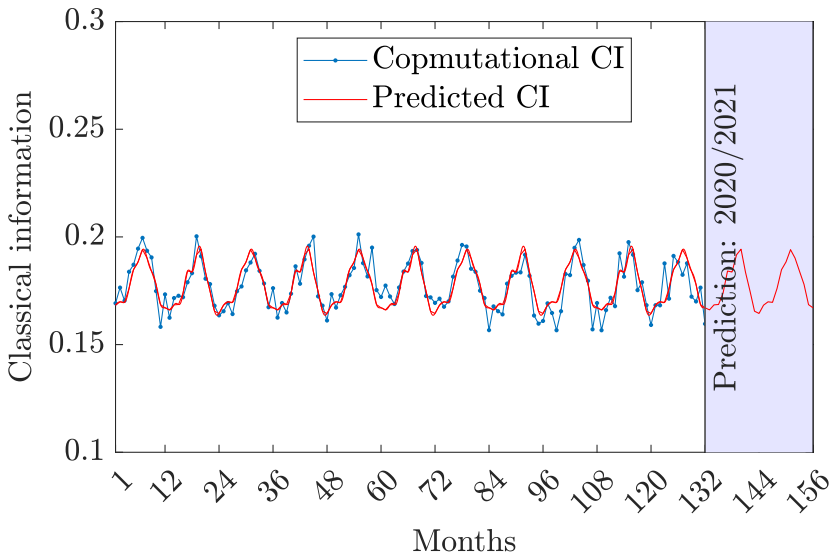

Figure 4. Computational and predicted classical information.

 doi:10.20944/preprints202502.1645.v1

In Figure 5, by Tables 3, 7 and 8 and Equation (20), the quantum information is plotted against months in two curves. The computational curve fluctuates far the predicted curve. The computational curve appears in an irregular behavior while the predicted curve has regular behavior. However, it depicts fluctuations in QI with no clear long-term increasing or decreasing trend.

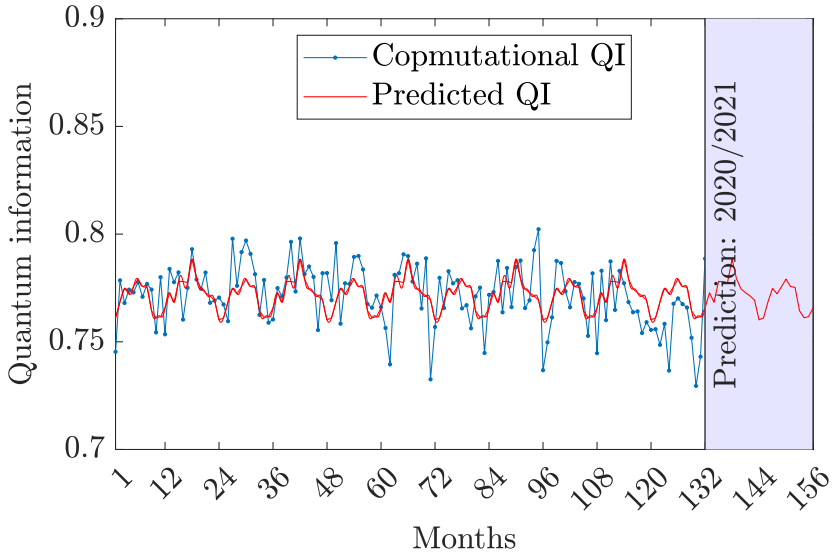

Figure 5. Computational and predicted quantum information.

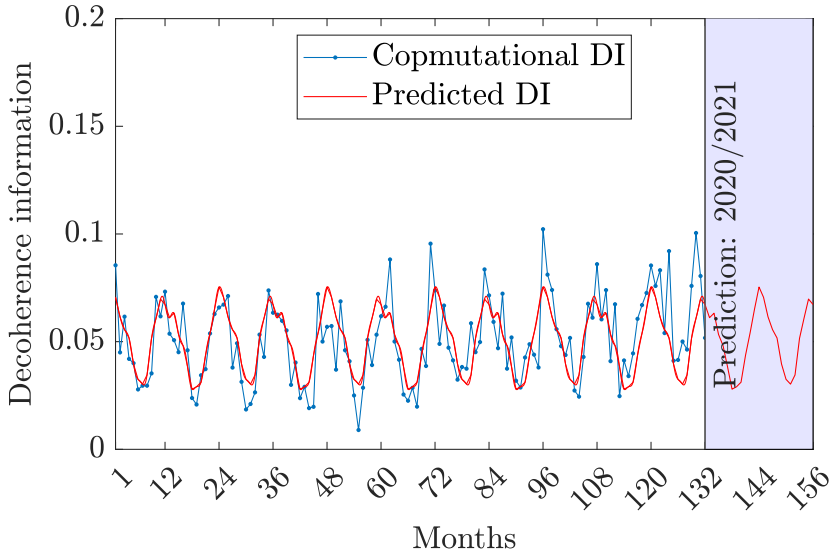

Figure 6. Computational and predicted decoherence information.

By Tables 4,7,8 and Equation (20), the decoherent information is provided graphically versus months by two curves in Figure 6. The computational curve undergoes slight fluctuations but the predicated curve is regular. Indeed, the system exhibits a high value of the quantum information relative to the classical information which means that the model behaves like a real quantum model rather than a classical one. When the information measures are compared; QI exhibits the highest value with respect to CI and DI. This proves that a treatment of the quantum mechanical system will provide with considerable information with respect to classical one.

Investigating two distinct types of entropy; S_H and S_N is shown in Figures 7 and 8 respectively. In Figure 7, Shannon entropy is plotted against months by Tables 5, 7 and 8 and Equation (20), in two curves. Clearly, the predicted curve is close to the computational curve with some slight fluctuations

 doi:10.20944/preprints202502.1645.v1

after $t > 84$. Shannon entropy describes a noise in the classical information with high values comparing with classical information values.

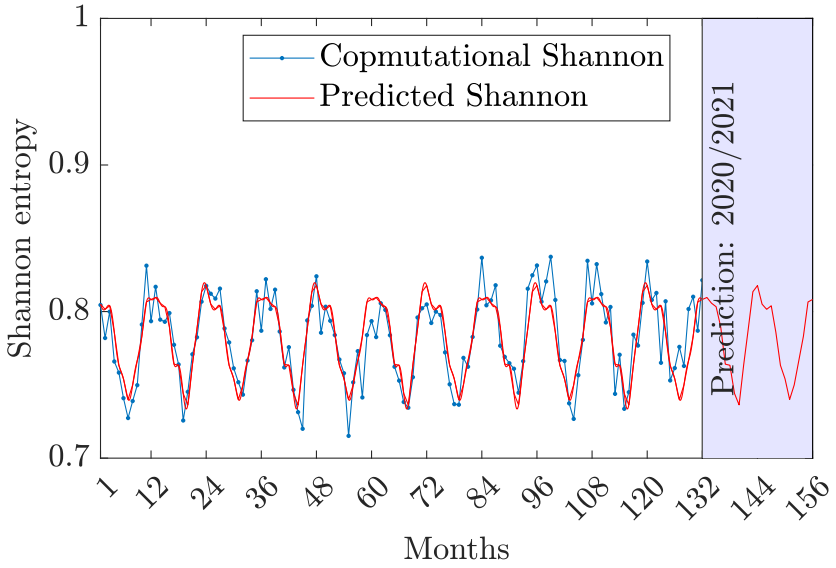

Figure 7. Computational and predicted Shannon entropy.

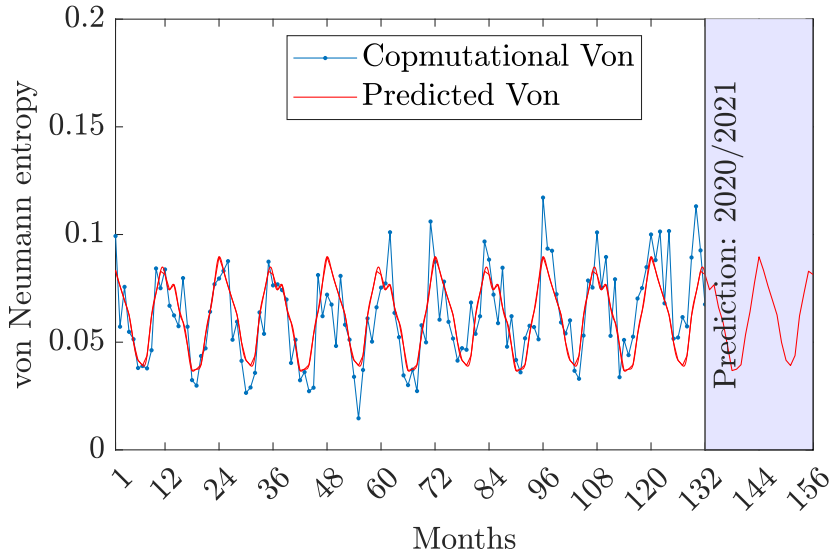

Figure 8. Computational and predicted Shannon entropy.

In Figure 8, von Neumann entropy is plotted against months by Tables 6–8 and Equation (20), in two curves. von Neumann entropy fluctuates in recent years and has small values which are near to values of the decoherent information. Indeed, the system exhibits a high value of Shannon entropy with respect to the von Neumann entropy approximately 10 times it. There is an oscillatory behavior in both measures due to the periodicity in weather dynamics. Measured values of von Neumann entropy prove the uncertainty of predicting the weather for a month relative to the Shannon entropy.

The analysis of Vancouver's weather dynamics from 2009 to 2019 through the lens of quantum information theory provides a unique perspective on climate data interpretation. Using concepts from various studies, such as the application of fuzzy logic in decision making [20] and the exploration of quantum entropy in physical systems [21,22], the research integrates advanced mathematical frameworks to model weather patterns. Additionally, insights from quantum classification algorithms [23,24] and the role of entanglement in complex systems [25–29] further enhance the robustness of this analysis. By synthesizing these diverse approaches, the study aims to reveal intricate relationships in

 doi:10.20944/preprints202502.1645.v1

weather dynamics, potentially leading to improved predictive models and a deeper understanding of climatic shifts in the Vancouver area.

5. Conclusions

In this paper, we investigated the weather dynamics of Vancouver based on quantum informative measures; the classical and the quantum and the decoherent information, Shannon and von Neumann entropies. We focus on the monthly mixed weather states. The quantum information is in the fornt and is followed by the classical information. The decoherent information occupies in the backyard. Thus, the model is treated in the quantum view since the quantum information is always greatest. Shannon and von Neumann entropies were studied here. It is reasonable that von neumann entropy cannot be neglected as it proves the uncertainity of predicting the weather dynamics for long-term period. We predicted quantum measures dynamics for the next two years and we calculated the errors for them during the compuational period base on a function reduced from Fourier series as function of fitting.

References

1. R. Mendelsohn, J. E. Neumann. The impact of climate change on the United States economy. Cambridge University Press, 2004.
2. J. B. Smith, D. A. Tirpak, The potential effects of global climate change on the United States: Report to Congress, Vol. 1, US Environmental Protection Agency, Office of Policy, Planning, and . . . , 1989.
3. L. Kalkstein, K. Smoyer, The impact of climate change on human health: some international implications, Experientia 49 (11) (1993) 969–979.
4. K. Charman, False starts and false solutions: current approaches in dealing with climate change, Capitalism Nature Socialism 19 (3) (2008) 29–47.
5. Adger, W. Neil, et al. "Adaptation to climate change in the developing world." Progress in development studies 3.3 (2003): 179-195.
6. Smit, Barry, and Olga Pilifosova. "Adaptation to climate change in the context of sustainable development and equity." Sustainable Development 8.9 (2003): 9.
7. Pecl, Gretta T., et al. "Biodiversity redistribution under climate change: Impacts on ecosystems and human well-being." Science 355.6332 (2017): eaai9214.
8. Field, Christopher B., and Vicente R. Barros, eds. Climate change 2014–Impacts, adaptation and vulnerability: Regional aspects. Cambridge University Press, 2014.
9. Von Storch, Hans, and Antonio Navarra, eds. Analysis of climate variability: applications of statistical techniques. Springer Science & Business Media, 1999.
10. Von Storch, Hans, and Francis W. Zwiers. Statistical analysis in climate research. Cambridge university press, 2002.
11. Bâra, Adela, Alin Gabriel Văduva, and Simona-Vasilica Oprea. "Anomaly Detection in Weather Phenomena: News and Numerical Data-Driven Insights into the Climate Change in Romania's Historical Regions." International Journal of Computational Intelligence Systems 17.1 (2024): 134.
12. C. E. Shannon, "A mathematical theory of communication," in The Bell System Technical Journal, vol. 27, no. 3, pp. 379-423, July 1948, doi: 10.1002/j.1538-7305.1948.tb01338.x.
13. Von Neumann, John. Mathematische grundlagen der quantenmechanik. Vol. 38. Springer-Verlag, 2013.
14. M. J. Reinsborough, A ricardian model of climate change in canada, Canadian Journal of Economics/Revue canadienne d économique 36 (1) (2003) 21–40.
15. N. Larsson. Adapting to climate change in canada, Building Research & Information 31 (3-4) (2003) 231–239.
16. H. Hengeveld, B. Whitewood, A. Fergusson, An introduction to climate change: A canadian perspective (2005).
17. F. Lenormand, C. R. Duguay, R. Gauthier, Development of a historical ice database for the study of climate change in canada, Hydrological Processes 16 (18) (2002) 3707–3722.
18. Leroyer, S., S. Blair, S. Z. Husain, and J. Mailhot, 2014: Subkilometer Numerical Weather Prediction in an Urban Coastal Area: A Case Study over the Vancouver Metropolitan Area. J. Appl. Meteor. Climatol., 53, 1433–1453, https://doi.org/10.1175/JAMC-D-13-0202.1.
19. Data link url: https://www.kaggle.com/datasets/luisvivas/weather-north-america?select=vancouver.csv.

20. Hamiden Abd El-Wahed Khalifa, Pavan Kumar, Bayoumi Ali Hassan, An Inexact Rough Interval of Normalized Heptagonal Fuzzy Numbers for Solving Vendor Selection Problem, Appl. Math. Inf. Sci. Volume 15, No. 3 PP: 317-324 (2021), doi:10.18576/amis/150309
21. Serkan Onar, Bayram Ali Ersoy, Kostaq Hila, Krisanthi Naka, (T,S)-Intuitionistic Fuzzy Hyperideals of $\Gamma-$Hyperrings, Appl. Math. Inf. Sci. Volume 15, No. 3 PP: 329-342 (2021), doi:10.18576/amis/150311
22. Abdalla, M.S., Obada, A.-S.F., Abdel-Aty, M. Von Neumann entropy and phase distribution of two mode parametric amplifier interacting with a single atom, Annals of Physics, 2005, 318(2), pp. 266–285 DOI: 10.1016/j.aop.2005.01.002
23. Obada, A.-S.F., Abdel-Aty, M. Influence of the stark shift and kerr-like medium on the evolution of field entropy and entanglement in two-photon processes, Acta Physica Polonica B, 2000, 31(3), pp. 589–599
24. Abdel-Aty, M., Furuichi, S., Obada, A.-S.F. Entanglement degree of a nonlinear multiphoton Jaynes-Cummings model, Journal of Optics B: Quantum and Semiclassical Optics, 2002, 4(1), pp. 37–43 DOI: 10.1088/1464-4266/4/1/306
25. Abdel-Aty, A.-H., Kadry, H., Zidan, M., Zanaty, E.A., Abdel-Aty, M. A quantum classification algorithm for classification incomplete patterns based on entanglement measure, Journal of Intelligent and Fuzzy Systems, 2020, 38(3), pp. 2817–2822 DOI: 10.3233/JIFS-179566
26. Khalida Inayat Noor, Muhammad Aslam Noor, Hamdy M. Mohamed, Quantum Approach to Starlike Functions, Appl. Math. Inf. Sci. Volume 15, No. 4 (2021) PP: 437-441 doi:10.18576/amis/150405
27. Amer Basim Shaalan, Nadir Fadhil Habubi, Sami Salman Chiad, Ziad Abdulahad Toma, New Design of Hairpin-Koch Fractal Filter for Suppression of Spurious Band, Int. J. Thin Film Sci. Tech. Vol. 2 No. 3 (2013) PP: 217-221
28. Alaa Zuhir Al Rawashdeh, Asma Rebhi Al Arab, Noura Nasser Alqahtani and Zineb Hadmer, The Sociological Understanding, for Corona Crises and its Reflections on Society: An Inductive Analytical Vision, J. Stat. Appl. Prob. Vol. 10, No. 1 (Mar. 2021), PP:267-286 doi:10.18576/jsap/100123
29. Yeqian Liu, Extended Bayesian Framework for Multicategory Support Vector Machine, J. Stat. Appl. Prob. 9 (2020) 1-11: doi:10.18576/jsap/090101